nature COMMUNICATIONS

ARTICLE

Received 23 Dec 2014 | Accepted 21 Jul 2015 | Published 9 Sep 2015

DOI: 10.1038/ncomms9117 OPEN

Sliding tethered ligands add topological interactions to the toolbox of ligand–receptor design

Martin Bauer[1,2], Patrick Kékicheff[1], Jean Iss[1], Christophe Fajolles[2], Thierry Charitat[1], Jean Daillant[2] & Carlos M. Marques[1]

Adhesion in the biological realm is mediated by specific lock-and-key interactions between ligand–receptor pairs. These complementary moieties are ubiquitously anchored to substrates by tethers that control the interaction range and the mobility of the ligands and receptors, thus tuning the kinetics and strength of the binding events. Here we add sliding anchoring to the toolbox of ligand–receptor design by developing a family of tethered ligands for which the spacer can slide at the anchoring point. Our results show that this additional sliding degree of freedom changes the nature of the adhesive contact by extending the spatial range over which binding may sustain a significant force. By introducing sliding tethered ligands with self-regulating length, this work paves the way for the development of versatile and reusable bio-adhesive substrates with potential applications for drug delivery and tissue engineering.

[1] Institut Charles Sadron, Université de Strasbourg, CNRS-UPR 22, 67034 Strasbourg Cedex, France. [2] CEA/ IRAMIS/SIS2M/LIONS, UMR 3299 CEA/CNRS, CEA-Saclay bâtiment 125, 91191 Gif-sur-Yvette Cedex, France. Correspondence and requests for materials should be addressed to C.M.M. (email: marques@unistra.fr).

The binding potential for the reaction between a ligand and its complementary receptor extends over a short microscopic length, typically a fraction of a nanometre[1], as for instance for the typical antigen–antibody bonds[2]. In natural and biomimetic systems, such short reaction ranges would be ineffective in driving adhesion between opposing surfaces, due to the reduced chances of encounter between the corresponding pair moieties. In practice, bio-adhesion requires a spacer, also called a tether, that governs the strength, the kinetics and the range of the binding events. While maintaining the physical attachment of the receptors or the ligands to the substrate, the tether increases the available phase space of their positions and orientations, markedly changing the kinetics and the effective interaction potential of the binding pairs[3]. Often built from a macromolecule, the tether can extend the interaction range between two opposing surfaces up to tens of nanometres, reshaping the surface interaction potential and controlling the final mechanics of adhesion buildup or detachment[4]. The tether is thus the unavoidable keystone of design when one seeks to tailor-make ligand–receptor pairs for specific adhesion[5].

Optimizing the tether architecture for binders operating between biological substrates under physiological conditions appears as an insuperable challenge. Indeed, the optimal distance from the anchoring surfaces for positioning the complementary ligands and receptors is not, for such substrates, a fixed quantity; it rather depends on time and surface coordinate. Simply choosing a single optimal architecture from the available tether spectrum that includes different lengths, rigidities or chemical moieties cannot in practice solve the design problem since it would require a spatial and temporal optimization of tether parameters[6]. We propose here to tackle this challenge, by introducing a family of spacers with self-adjustable contour length that we coined sliding tethered ligands (STLs). On the basis of topological complexes between polyethylene glycol (PEG) and cholesteryl α-cyclodextrins (CDs), which can be inserted into phospholipid membranes due to their cholesteryl anchor[7,8], STLs combine a ring-shaped anchor through which a polymer chain can slide, while polymer escaping from the ring is prevented by end-attached ligands. Theoretical work on these sliding polymer tethers suggests that they are able to adapt their conformation to external conditions[9], the sliding character of the topological complex formed by the polymer and the ring is expected to translate into more effective binding and smoother adhesive detachment.

Results

The system and experimental setup of this work is shown in Fig. 1. STLs were synthesized (Supplementary Fig. 1) with a PEG tether ($\bar{N} = 222$) threaded through the cavity of a cholesteryl α-CD and end-capped with adamantane at both chain ends (Fig. 1a). Since adamantane forms a host–guest complex with β-CD[10,11], we also synthesized a cholesteryl β-CD (Fig. 1b and Supplementary Fig. 2), as the receptor. Both the STLs and the cholesteryl β-CDs, at equal surface densities, are inserted into opposing phospholipid membranes (Fig. 1c) by their cholesteryl moieties. The synthesis of all compounds is described in the Supplementary Methods.

Controlling surface structure of STLs and cholesteryl β-CD. We studied bilayers modified with STL, as well as cholesteryl β-CD in water with the exact same molecular configuration and with the same chemicals used for the force experiments described below. Figures 2a and 3a display the reflectivity curves for both bilayer samples obtained for three different contrasts and the corresponding best coupled fits. The resulting scattering length density profiles with the schematic structure of the bilayers are shown in Figs 2b and 3b. The fitted parameters are listed in Supplementary Table 4. The DSPE headgroup layer close to the silicon substrate is in good agreement with data already reported in literature[2,12]. We found a hydrophobic tail layer thickness of 3.9 nm for the bilayer modified with STL and slightly smaller thickness for the cholesteryl β-CD layer. The measured thicknesses and scattering length densities (SLDs; $-0.3\ \text{Å}^{-2}$) are as expected for a hydrophobic core in gel phase composed of DSPE and DPPC tails[13,14]. A low water content of ca. 10% had to be added due to holes in the bilayer. The presence of the STL and the cholesteryl β-CD in the outer mixed headgroup region leads to a slightly increased thickness compared with the bare DPPC layer (1 nm compared to 0.9 nm for pure DPPC). For the STL bilayer we obtained a polymer layer with a height $h = 13$ nm and a surface density $\sigma = 0.051\ \text{nm}^{-2}$ that are in good agreement with the ones obtained from force experiments as described below.

Surface force interactions. Force–distance profiles between the two opposing surfaces displayed in Fig. 1 were measured by the surface force apparatus (SFA) technique[15] directly after film buildup. As the separation between the surfaces decreases, the forces increase steadily, revealing three distinct regimes in the force–distance profile shown in Fig. 4. Reversible force profiles are observed on compression or separation, as long as the two opposite surfaces do not come into contact (surface separations larger than ~ 20 nm). At these large separations, the fully reversible repulsion decays exponentially with a large decay length, $\kappa^{-1} = 110$ nm, close to the Debye screening length expected for pure water in equilibrium with dissolved carbonic gas, at pH 5.7. The repulsive forces result from the overlap of the electrical double layers associated with the charged polar heads of the phospholipids. At short approaching distances (< 20 nm), the electrical double-layer repulsion is dominated by a steeper repulsion due to the compression of the confined polymer brush. Ultimately, there is a marked change in the repulsive force profile towards a steeper regime at very small separations, which may be ascribed to the steric wall repulsion. Indeed, the primary adhesive minimum observed for bare mica surfaces in air or water can no longer be observed. Comparison with the bare mica contact position leads to a value of 9.8 ± 0.2 nm for the thickness of the two lipid bilayers, a value taken hereafter as the zero reference distance for all force–distance profiles. The forces generated by the sliding tethered ligands can be obtained by subtracting the DLVO (Derjaguin-Landau-Verwey-Overbeek) contribution from the force curves displayed in Fig. 4. They are comprised of a repulsive part due to the compression of the polymer spacers and of an attractive component due to sliding ligand forces as demonstrated below.

Ruling out nonspecific interactions. To rule out unspecific adhesion, we performed two reference experiments. In both experiments we have used the exact same amounts of STL and cholesteryl β-CD, as for the main experiment. Figure 5 shows the force curves between one DPPC bilayer modified with STL and the opposing bilayer consisting of pure DPPC. They display the steric repulsion due to the polymer compression. As expected[2,16], no adhesive regime was observed for approach as well as withdrawal. Figure 6 displays the reference experiment with one DPPC bilayer modified with the surface density of cholesteryl β-CD. On withdrawal the curves exhibited a very short-ranged adhesion that is due to van der Waals adhesion, which is in good agreement with experiments for pure lipid bilayers previously described in the literature[17].

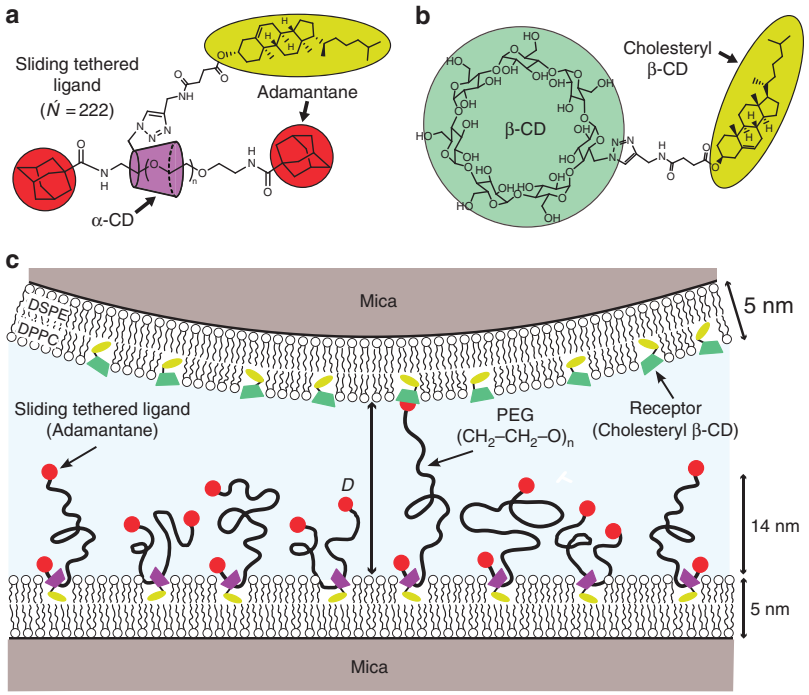

Figure 1 | Experimental geometry. (**a**) Molecular structure of a STL. (**b**) The cholesteryl β-CD receptor. (**c**) Molecular configuration used in the SFA experiments. Both membranes deposited on mica by a Langmuir–Blodgett technique were in a gel phase so as to minimize lateral mobility. The surface number density of STLs was $\sigma = 0.044\,\mathrm{nm}^{-2}$, which corresponds to $23\,\mathrm{nm}^2$ for each tethered ligand molecule (94:6 DPPC:STL). The STLs formed a polymer brush of mean thickness $h_0 = 14$ nm, as determined from SFA compression curves and confirmed by neutron reflectivity experiments. Each STL is composed of a PEG polymer ($\bar{N} = 222$), which is threaded through the cavity of a cholesteryl α-CD membrane anchor and capped with adamantane at each end. There are on average 1.8 cholesteryl α-CD anchors per chain, as determined by nuclear magnetic resonance. In the opposing surface the ratio DPPC:cholesteryl β-CD is 90:10. The distance between opposing surfaces, *D*, is referred to and measured from the outer edge of the lipid head groups.

Repulsion from the compressed spacers. Figure 7 shows the polymer compression forces under approach, F_{rep}, extracted from both the adhesive geometry and the non-adhesive case where the top layer does not carry cholesteryl β-CD. We follow the method and notations of Balko *et al.*[18] that implemented the Milner–Witten–Cates model[19,20] to fit the force profiles under approaching conditions. Experiments and theory (full lines) are in excellent agreement over a large range of compressions, from the onset of the repulsion, where the repulsive forces vanish, up to high compressions at small distances. With the given polydispersity index = 1.25, one obtains a brush height $h_0 = 14$ nm, corresponding to a STL surface number density $\sigma = 0.044\,\mathrm{nm}^{-2}$ using an ethylene glycol monomer size $a = 3.5$ Å (ref. 21), which is close to the number density measured by neutron reflectivity[22] (see also Supplementary Table 2).

Specific adhesion forces resulting from ligand sliding. The forces under separation are shown in Fig. 8. At short distances the forces are repulsive but become attractive as the separation distance increases. Note that the attractive profile does not present a dependence on the resting time at contact under an applied load (up to a few hours at fixed load) nor on the number of cycles (load/unload) previously performed at the same contact position. Attraction is due to the bridging forces induced by the specific binding between the adamantane end group of the tethers and the β-CD receptor on the opposing surface. Indeed, as shown above, no attractions are observed in the absence of either the functional adamantane chain end or the β-CD groups. The amplitude of the attraction increases as the minimum distance of approach decreases, as one would expect from the evolution of the bridging probability as a function of minimum approach distance, D^{min}.

Discussion

Attractive forces due to tethered ligand–receptor interactions have been previously observed and quantitatively explained by a combination of polymer and ligand binding theories[2,3,21,23,24]. However, the actual force profiles of Fig. 8 present marked differences with the usual U-shaped profiles of such systems[2,3]—see Fig. 8 and Supplementary Fig. 3 for the non-sliding profile expected in our case—suggesting a subtle role of the sliding character of our tethers. To quantitatively explain the STL force profiles we write the STL contribution to the total force *F* between the two SFA surfaces of radius of curvature *R* as the sum of the repulsive component measured and analysed beforehand, F_{rep}, and all attractive contributions from the individual chains as:

$$F = F_{\mathrm{rep}} - 2\pi R\left\{\sigma_N \int_D^\infty \mathrm{d}h f_N(h)\rho_N(h) + \sigma_{\frac{N}{2}} \int_D^\infty \mathrm{d}h f_{\frac{N}{2}}(h)\rho_{\frac{N}{2}}(h) - \sigma_{\frac{N}{2}} \int_D^\infty \mathrm{d}h f_0 \rho_{\frac{N}{2}}(h)\rho_N\left(h + D - D^{min}\right)\right\} \quad (1)$$

where σ_N and $\sigma_{\frac{N}{2}}$ are, respectively, the surface densities of single-end and double-end bridges that we refer to as strands and loops (see right panels in Figs 8 and 9), $f_{\frac{N}{2}}$ and f_N are, respectively, the attractive forces exerted by the loops and the strands, f_0 is a constant force required to pull the chains through the CD rings, and $\rho_{\frac{N}{2}}$ and ρ_N are cutoff functions accounting for the dissociation of the adamantane/β-CD host–guest complex. The three

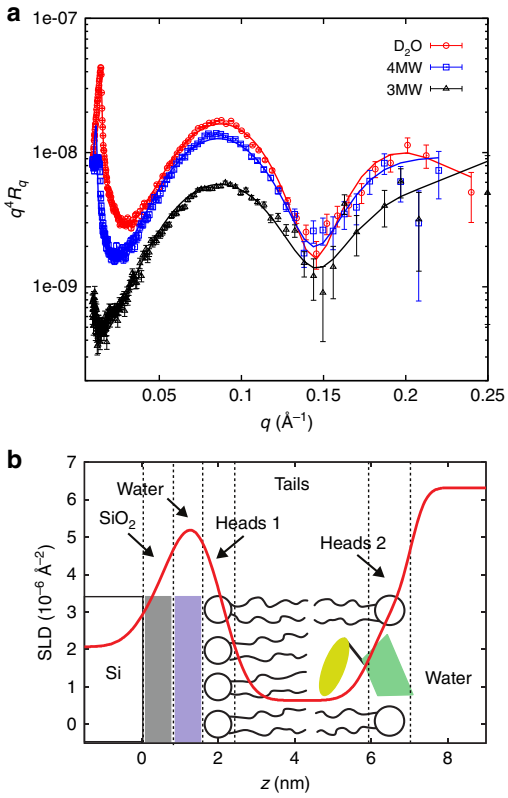

Figure 2 | Structure of bilayer with anchored receptors. (**a**) Neutron reflectivity curves for supported bilayer on silicon consisting of a first monolayer DSPE and a second DPPC monolayer with inserted cholesteryl β-CD at 25 °C in water recorded for three different subphase contrasts. (**b**) Corresponding scattering density layer profile obtained with a five-layer fitting model as indicated schematically.

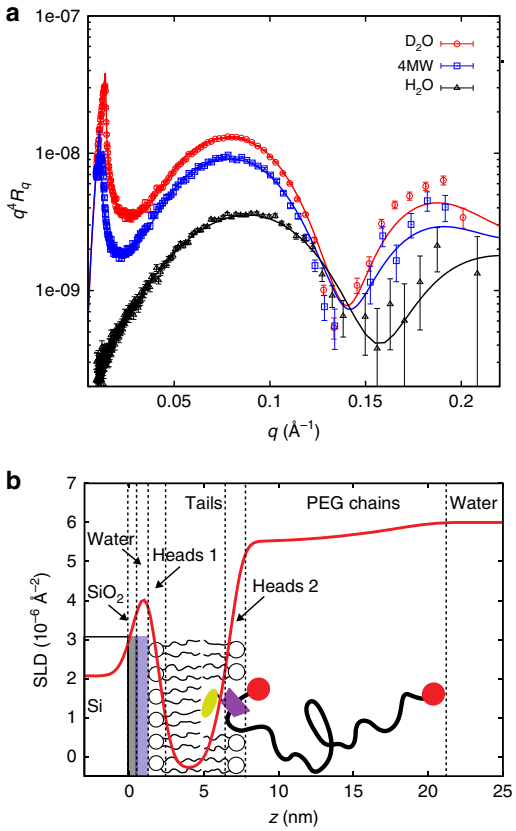

Figure 3 | Structure of bilayer with anchored STLs. (**a**) Neutron reflectivity curves for supported bilayer on silicon consisting of a first monolayer DSPE and a second DPPC monolayer with inserted STL at 25 °C in water recorded for three different subphase contrasts. (**b**) Corresponding scattering density layer profile obtained with a six-layer fitting model as indicated schematically.

attractive terms of this equation correspond to the three regions in Fig. 9. The first term refers to the attractive forces of single strands, the second term the attractive forces of loops and the third term the forces generated by the interconversion mechanism. For the strands bridging between opposite walls at distance h, we consider forces and ranges of attraction described by:

$$f_N = K_N\,(h - h_N);\ \rho_N = \frac{1}{1+\exp\left[\frac{1}{2}K_N(h-h_N)^2 - E_L\right]} \qquad (2)$$

where the forces f_N are in practice given by harmonic spring contribution with a spring constant $K_N = \frac{25}{aN^{1.46}}$ and an equilibrium position $h_N = 1.05aN^{0.65}$ with $a = 0.35$ nm. The values of K_N and h_N were obtained by numerical simulations and shown before to adequately describe stretching of polymer chains with the distance range relevant for our experiments[3]. Given the ligand–receptor band strength E_L (here $E_L = 10$ in k_BT units, calculated from the binding constant $5\times10^4\,M^{-1}$ (refs 10,11,25)) the function ρ_N measures the thermally activated detachment of strands when the stretching energy $\frac{1}{2}K_N(h-h_N)^2$ becomes larger than the bond strength E_L. Forces and range of attraction for bridging loops are described likewise with a monomer number $N/2$ in the equation (2). When one extremity of a bridging loop detaches, the force balance between the two loops halves does not hold any longer, and half of the chain may be pulled through the anchoring CD ring until eventually sliding is prevented by the tether capping moiety. Our fitting shows that the polymer chain does not slide freely through the anchoring ring, but instead a finite force is required to pull the PEO chain through the CD ring. We have modelled this finite force as being constant, f_0, throughout the sliding process. During interconversion, where a freshly detached loop is being stretched until it eventually becomes a strand, its contribution to the total force is described by the third attractive term of equation (1) with ρ_N and $\rho_{\frac{N}{2}}$ given by equation (2) with N and $N/2$, respectively. The product of distributions ρ_N and $\rho_{\frac{N}{2}}$ in the third term counts chains freshly detached for distances larger than $D^{max}_{N/2}$ and not yet reaching the 'strand state' at distances $D^{max}_{N/2} + D - D^{min}$.

Fittings of all curves in Fig. 8 were made with a fixed set of parameters, except for the initial relative fraction of bridging loops and strands, indicated in the inset. The quality of the fitting procedure convincingly shows that interconversion between loops and strands, pictured on the right panel of Fig. 8 and assumed for writing equation (1), does indeed control the attractive forces in the STL system. In the interconversion scenario, the initial bonding state of the sliding tethers consists of a mixture of single bridges (the strands), double bridges (the loops) and unbound chains. As the two opposing surfaces are pulled apart, the loops are progressively converted into strands due to the rupture under force of one of the adamantane/β-CD bonds. A freshly ruptured loop is then pulled at constant force f_0 through its CD ring, eventually detaching when the stored stretching energy becomes

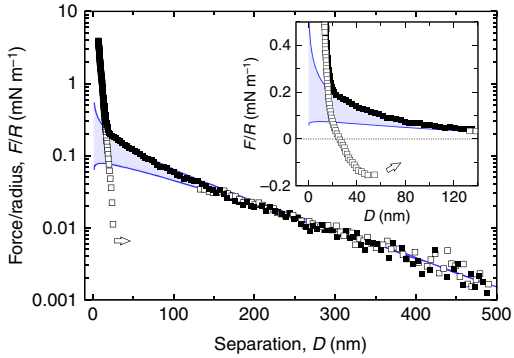

Figure 4 | Total surface forces. Measured forces, *F*, normalized by the mean radius of curvature of the surfaces, *R*, between the functionalized bilayers of Fig. 1, as a function of surface separation, *D*. Solid symbols (■) describe forces on approach and open symbols (□) the corresponding forces on separation. The upper and lower solid lines are fits from a DLVO model[34,35] with, respectively, a constant surface charge σ_0 or a constant surface potential Ψ_0 boundary conditions (best fit gives $\sigma_0 = 28\,\mu C\,m^{-2}$; $\Psi_0 = 44$ mV). The electrostatic component of the DLVO model is computed from numerical solutions of the nonlinear Poisson–Boltzmann equation[36] and the attractive van der Waals force is obtained with a calculated non-retarded Hamaker constant $A_{121} = 1 \times 10^{-20}$ J using the Lifshitz theory[37]. Note that the DLVO fit is constrained by the long-range exponential nature of the force profile at large separation distances, with a Debye screening length $\kappa^{-1} = 110$ nm. At small separations the force-distance profile deviates significantly from the predicted electrostatic repulsion due to the compression of the STL brush. Furthermore, at such strong compressions, the forces acquire an irreversible component and eventually a pull-off force must be applied to wrench the surfaces apart (arrows), as better seen in the linear scale plot of the inset.

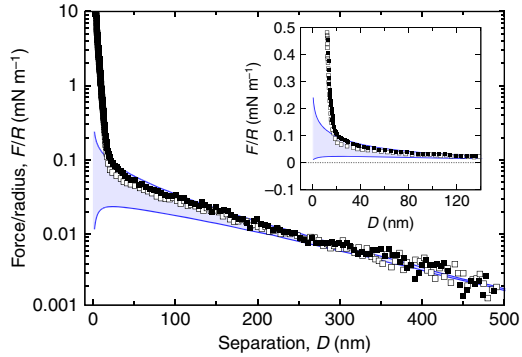

Figure 5 | Reference forces between STLs and a surface without receptors. Normalized force-distance profiles between a bilayer modified with STLs and a pure DPPC bilayer on approach (■) and separation (□) of the surfaces. At large separations the interaction is exponentially repulsive as expected for a double-layer interaction. Solid lines represent the boundary conditions constant surface charge σ_0 (upper curve) and constant surface potential Ψ_0 (lower curve) calculated as before. The best-fit parameters, $\Psi_0 = 30$ mV and $\kappa^{-1} = 150$ nm, are essentially constrained by the long-range exponential repulsive part of the force profile. The inset shows an enlargement of the force-distance profile on a linear scale at short separations. It indicates that the electrical double-layer repulsion operates at almost constant surface charge boundary conditions. At short separations the interaction deviates from the pure electrostatic repulsion due to the compression of the STL chains. When compressing further the surfaces a steric repulsion due to the deposited bilayers on the mica substrates is ultimately encountered. No attractive component is observed when the surfaces are separated (□) even under large applied loads: the observed small hysteresis here reported simply indicates that the local structure has been slightly affected under such conditions.

comparable with the binding energy of ligand–receptor, about $10\,k_BT$ units[11,25]. Pulling the chains through the rings at constant force is essential to describe the nearly linear decay that precedes the minima of the attractive force profiles in Fig. 3. Such decay is not present in a typical attractive profile for tethered ligand–receptor pairs[2,3], also depicted in Fig. 8. Note that the minima of the measured forces in our case are located at about the same separation indicating that, from the polydisperse composition of chain lengths, chains of $N = 600$ contribute most to the withdrawal force profiles. The shapes of attractive profiles measured for STLs are in marked contrast with attractive forces resulting only from chain stretching (Fig. 8 and Supplementary Fig. 3): they provide in practice for a long-range, smoother force profile between the complementary surfaces. To our knowledge this is a new feature for bio-adhesive attractive profiles, observed for the first time here with our STL system.

We have thus designed and built a new family of sliding tethered ligands. The goal of spacer design is to facilitate the formation of the ligand–receptor bond, by attaching the ligand or the receptor to a flexible or semiflexible tether, which enhances the conformational space for ligand orientation[26] and position[3]. An intrinsic limitation of conventional spacer design with a fixed length is that one typically optimizes spacer length according only to the particular nature of a given adhesion system in drug delivery or tissue engineering. Here, by anchoring the spacer to the substrate with a sliding connection, we effectively provide for a large number of possible spacer lengths within the same molecular architecture. As we have shown, this changes the intimate force profile of the adhesive contact, paving the way for the development of new, more effective and versatile bio-adhesive substrates.

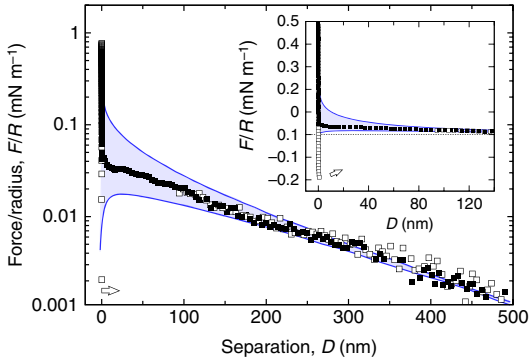

Figure 6 | Reference forces between the receptors and a naked bilayer. Normalized force-distance profiles between a bilayer modified with cholesteryl β-CD and a pure DPPC bilayer on approach (■) and separation (□) of the surfaces. At large separations the interaction is exponentially repulsive as expected for a double-layer interaction. Solid lines are calculated as described before at constant surface charge and constant surface potential boundary conditions with $\Psi_0 = 25$ mV and $\kappa^{-1} = 150$ nm. At short separations the repulsion deviates from the pure electrostatics as a steric repulsion due to the presence of the deposited bilayers on mica is encountered. A small pull-off force must be applied to separate the surfaces at contact (arrow): its range and magnitude indicate van der Waals interactions.

Methods

Chemicals. STLs and the cholesteryl β-CD were synthesized in our group, as described in Supplementary Methods, see also Supplementary Table 1 for chemicals used in this work. For STL, we use a PEG tether ($\bar{N} = 222$) threaded

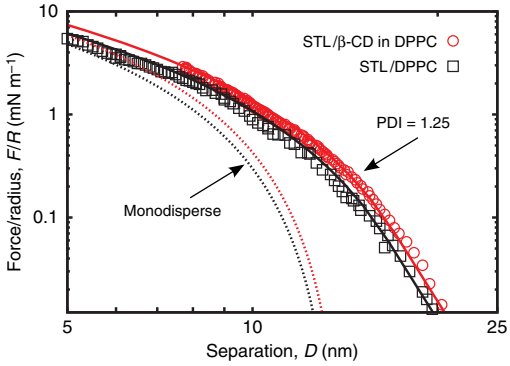

Figure 7 | Net repulsive forces induced by STLs on a naked bilayer without receptors. Approach curves after subtraction of the constant charge DLVO contribution, for the sample architecture displayed in Fig. 1 and for the reference experiment with the same STL content but without cholesteryl β-CD receptor. The dashed lines correspond to Milner–Witten–Cates (MWC) fits[18–20] for monodisperse polymers. The full lines represent MWC fits numerically corrected for polydispersity (polydispersity index = 1.25). As expected we find similar brush heights for both samples: $h_0 = 13.8 \pm 0.5$ nm without β-CD and 14.2 ± 0.5 nm with β-CD.

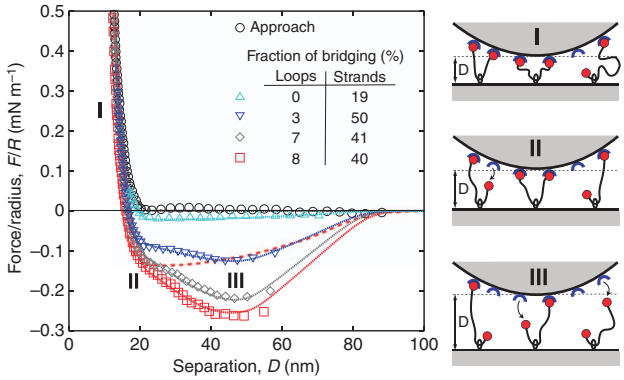

Figure 8 | Net attractive forces induced by STLs mediated specific interactions. Force profiles obtained on approach (circles) and on separation (all other symbols) after subtraction of DLVO contribution on the same sample spot successively increasing the compression on approach. The full lines represent fits of the force profiles according to the model described by equation (1) with parameters summarized in Supplementary Table 3. The coarse dashed line represents the expected attraction curves without interconversion, for the same total number of bridges as the red curve (squares). On the right hand one can find a schematic illustration of the proposed mechanism for the interconversion of double-bridging STLs into single-bridging STLs, responsible for the unique force profiles.

through the cavity of a cholesteryl α-CD and end-capped with adamantane at both chain ends. The DPPC (1,2-dipalmitoyl-sn-glycero-3-phosphocholine), DSPE (1,2-distearoyl-sn-glycero-3-phosphoethanolamine) chloroform (stabilized with ethanol) were purchased from Sigma–Aldrich. The ultra-pure water (18.2 MΩ cm) was obtained from a commercial Millipore purification system.

Surface force apparatus experiments. The solid support consists of thin, molecularly smooth, back-silvered mica sheets, glued onto fused silica hemi-cylinders with an average radius of curvature $R \approx 2$ cm. After thickness calibration of the mica sheets, the bilayer samples are prepared by Langmuir–Blodgett deposition. A chloroform–methanol 4:1 solution of lipids, lipid–STL or lipid–CD was spread on the water surface of a Langmuir NIMA trough (10 cm × 30 cm). The isotherms are recorded with a speed of 10 cm^2 min^{-1} at 25 °C. All samples are prepared with a first layer of DSPE, deposited at 40 mN m^{-1} as a 65:35:8 chloroform:methanol:water solution spread on the water surface. The second

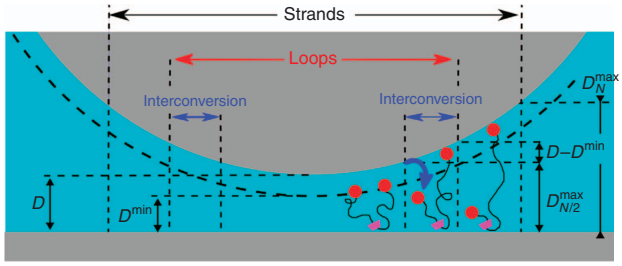

Figure 9 | Schematics of bond interconversion. For opposite curved surfaces separated by a distance D, bridging loops can exist only in the central region of the gap provided the distance between the anchoring ring and the ending caps is smaller than $D_{N/2}^{max}$ while bridging single strands may exist up to separations D_N^{max}. When the two opposite surfaces are separated from the minimal separation D^{min} set after brush compression, one extremity of a bridging loop will detach as soon as the distance between its anchoring ring and one of its extremity becomes larger than $D_{N/2}^{max} + D - D^{min}$; in this namely 'interconversion zone' this former bridging loop has been transformed into a new single strand. In this schematic all the other STLs of the brush, which are not bridging the two opposite surfaces, have not been represented for clarity.

layer is always deposited at 30 mN m^{-1} and degased ultra-pure water is used as subphase. The deposition speed is set to 5 mm min^{-1} for the DSPE layer and to 2 mm min^{-1} for the second layer. The transfer ratios have been close to one for the first layer and >0.9 for the second layer.

All force measurements were performed at 25.0 °C with mica surfaces coated with freshly deposited bilayers. The films were studied in pure degased millipore water and kept in aqueous environment at all times to preserve their native structural organization. Force–distance profiles were measured using a home-made device based on the initial version of the Tabor–Israelachvili SFA[15]. As described in detail elsewhere[27] the instrument allows the force F between two mica surfaces (of mean radius of curvature R) to be measured to within 10 nN as a function of the determined surface separation D, which can be measured to a typical accuracy of 0.2 nm, using multiple beam interferometry[28]. The normalized force F/R can be detected to within 0.003 mN m^{-1}, while the maximum reliably measurable force will depend on the mechanical compressibility of the entire system. Typically surface deformations occur for applied loads larger than 8–15 mN m^{-1} and F/R becomes meaningless due to the deformation of the glue beneath the mica sheet; for that reason, data are only reported for smaller loads, where the measured values of F/R correspond to the free energy E per unit area[29]. Highly reliable results were obtained by performing measurements under negligible thermal drift between the surfaces, below 0.5 nm min^{-1}, it is minutes to the power minus one, at several different contact positions. To maximize the time for achievement of thermodynamic equilibrium, the surface displacements were carried out as slowly as any thermal drift would permit.

Neutron reflectivity. *Sample preparation.* The bilayers were prepared on 5 × 5 × 1 cm^3, homogeneously n-doped silicon single crystals, oriented [111] on the side where the film is deposited and atomically smooth with a roughness <5 Å, as determined by the manufacturer (SILTRONIX, Archamps, France). Before each deposition the silicon block was cleaned with chloroform, ethanol and water then treated with ultraviolet/ozone for 30 min to reach a hydrophilicity as high as possible. The double-layer deposition was carried out on a NIMA trough available in the ILL soft matter lab (20 × 30 cm^2). The first layer of DSPE was deposited at 40 mN m^{-1} by the classical Langmuir–Blodgett technique, whereas the second layer of DPPC, modified either with STL or cholesteryl β-CD, was deposited by the Langmuir–Schaefer method (horizontal sample) at 30 mN m^{-1}. The temperature was kept constant at 25 °C. The samples were then inserted into a Teflon sample cell, which was put into an aluminium box to be mounted on the neutron reflectometer and temperature controlled using a water circulation bath. The cell was connected to a solvent circuit by means of a peristaltic pump to be able to change the subphase for different contrast. More detailed information about the substrate and sample preparation has been given elsewhere[13].

Instrumental setup. The measurements were conducted at the D17 reflectometer[30] operated in time of flight mode at the ILL, Grenoble (France) with a wavelength range from 2 to 20 Å, giving a q-range for specular reflectivity of 0.005–0.3 Å^{-1}. Each measurement is performed at two reflection angles, $\theta_1 = 0.8°$ (resolution $\Delta q/q = 2.7\%$) and $\theta_2 = 3.2°$ (resolution $\Delta q/q$ varied linearly from 3.8 to 13%) (ref. 30). The detector efficiency was calibrated with H_2O. For the actual experiment the neutron beam enters the silicon substrate through one 5 × 1 cm^2 side of the block, hits at grazing incidence the polished 5 × 5 cm^2 face on which the

layer under study has been deposited, and goes out through the opposite $5 \times 1\text{-cm}^2$ side[13]. Two direct beams have been measured at the settings of the two angles of incidence for data normalization. Each sample was measured at three different solvent contrasts, such as H_2O (SLD $= -0.56 \times 10^{-6}$ Å^{-2}), 4-match water (4MW, SLD $= 4 \times 10^{-6}$ Å^{-2}) and D_2O (SLD $= -6.4 \times 10^{-6}$ Å^{-2}) to remove ambiguities of the fits[13,31].

Data analysis and fitting model. Specular reflectivity, $R(q)$, is defined as the ratio between the specularly reflected and incoming intensities of a neutron beam, which is measured as a function of the wave vector transfer, $q = \frac{4\pi}{\lambda}\sin\theta$, perpendicular to the reflecting surface, where θ is the angle and λ the wavelength of the incoming beam. $R(q)$ is related to the scattering length density profile across the interface by the square modulus of its Fourier transform. Therefore, the phase is lost and the data need to be fitted with an appropriate model to obtain the density profile. In this manner it is possible to determine film profiles within subnanometer precision[13,32]. The data are fitted with the ProFit package 6.2 (QuantumSoft), where the specular reflectivity is calculated by the Abeles matrix method for stratified interfaces[33].

For the cholesteryl β-CD/phospholipid bilayer a five-layer model has been adopted, which has already been used to describe bilayers with amphiphilic CDs[8], whereas for the STL/phospholipid bilayer sixth layer had to be added to account for polymer[22]. As illustrated by the cartoon in Fig. 2, they both consist of a SiO_2 layer on the silicon block, a thin water layer, a thin DSPE headgroup slab, a hydrophobic layer composed of phospholipid tails and the cholesteryl residues, as well as an outer DPPC headgroup slab with inserted CD moieties. For the STL bilayer an additional sixth layer with a parabolic density profile was added, widely used to model polymer brushes[2,19,20].

The fits for different contrasts have been performed in a coupled manner. Only the subphase scattering length density is changed for different contrasts. The error bars are determined by varying each parameter of the model and evaluating the χ^2 parameter, as well as visually checking the quality of the fit. The results fall within the error bars if they still give satisfactory fits for all measured contrasts. Good coupled fits could be obtained for all measured samples at different temperatures with an exploitable q-range from 0.01 to 0.25 Å^{-1}. The detailed fitting results can be found in the Supplementary Table 4.

Silicon substrates were first characterized, leading to a SiO_2 layer, 0.8-nm thick with a roughness of 0.6 nm. These parameters have been constrained to these values for fitting the supported bilayer experiments. For both samples we found a thin water layer with high roughness between substrate and the supported bilayer, which were in good agreement with literature values[13,32].

The surface density of the polymer σ was be calculated from the volume density profile $\Phi(h) = \int_0^h \Phi_0[1 - (\frac{Z}{h})^2]dZ$ with the brush thickness h and the polymer volume fraction at the interface Φ_0, which are both obtained as independent fit parameters from the neutron reflectivity experiments, using $\sigma = \Phi(h)/Nv_{EG}$ with the number of monomers N and the molecular volume of an ethylene glycol unit $v_{EG} = 0.061$ nm^3 (ref. 12).

References

1. Bongrand, P. Ligand-receptor interactions. *Rep. Progr. Phys.* **62,** 921–968 (1999).
2. Moore, N. W., Mulder, D. J. & Kuhl, T. L. Adhesion from tethered ligand-receptor bonds with microsecond lifetimes. *Langmuir* **24,** 1212–1218 (2008).
3. Jeppesen, C. *et al.* Impact of polymer tether length on multiple ligand-receptor bond formation. *Science* **293,** 465–468 (2001).
4. Moreira, A. G. & Marques, C. M. The role of polymer spacers in specific adhesion. *J. Chem. Phys.* **120,** 6229–6237 (2004).
5. Leckband, D. Design rules for biomolecular adhesion: lessons from force measurements. *Annu. Rev. Chem. Biomol. Eng.* **1,** 365–389 (2010).
6. Onyskiw, P. J. & Eniola-Adefeso, O. Effect of PEGylation on ligand-based targeting of drug carriers to the vascular wall in blood flow. *Langmuir* **29,** 11127–11134 (2013).
7. Klaus, A. *et al.* Amphiphilic behavior and membrane solubility of a dicholesteryl-cyclodextrin. *Langmuir* **27,** 7580–7586 (2011).
8. Bauer, M., Charitat, T., Fajolles, C., Fragneto, G. & Daillant, J. Insertion properties of cholesteryl cyclodextrins in phospholipids membranes: a molecular study. *Soft Matter* **8,** 942–953 (2012).
9. Baulin, V. A., Johner, A. & Marques, C. M. Sliding grafted polymer layers. *Macromolecules* **38,** 1434–1441 (2005).
10. Komiyama, M. & Bender, M. L. Importance of apolar binding in complex formation of cyclodextrins with adamantanecarboxylate. *J. Am. Chem. Soc.* **100,** 2259–2260 (1978).
11. Auletta, T. *et al.* ß-Cyclodextrin host-guest complexes probed under thermodynamic equilibrium: thermodynamics and AFM force spectroscopy. *J. Am. Chem. Soc.* **126,** 1577–1584 (2004).
12. Bianco-Peled, H. *et al.* Structural study of langmuir monolayers containing lipidated poly(ethylene glycol) and peptides. *Langmuir* **17,** 6931–6937 (2001).
13. Charitat, T., Bellet-Amalric, E., Fragneto, G. & Graner, F. Adsorbed and free lipid bilayers at the solid-liquid interface. *Eur. Phys. J. B* **8,** 583–593 (1999).
14. Watkins, E. B. *et al.* Structure and thermodynamics of lipid bilayers on polyethylene glycol cushions: fact and fiction of PEG cushioned membranes. *Langmuir* **27,** 13618–13628 (2011).
15. Israelachvili, J. N. & Adams, G. E. Measurement of forces between two mica surfaces in aqueous electrolyte solutions in the range 0-100 nm. *J. Chem. Soc. Faraday Trans. I* **74,** 975–1001 (1978).
16. Moore, N. W. & Kuhl, T. L. Bimodal polymer mushrooms: compressive forces and specificity toward receptor surfaces. *Langmuir* **22,** 8485–8491 (2006).
17. Marra, J. & Israelachvili, J. N. Direct measurements of forces between phosphatidylcholine and phosphatidylethanolamine bilayers in aqueous electrolyte solutions. *Biochemistry* **24,** 4608–4618 (1985).
18. Balko, S. M. *et al.* Polymer brushes under high load. *PLoS ONE* **8,** 0058392 (2013).
19. Milner, S. T., Witten, T. A. & Cates, M. E. Theory of the grafted polymer brush. *Macromolecules* **21,** 2610–2619 (1988).
20. Milner, S. T., Witten, T. A. & Cates, M. E. Effects of polydispersity in the end-grafted polymer brush. *Macromolecules* **22,** 853–861 (1989).
21. Wong, J. Y., Kuhl, T. L., Israelachvili, J. N., Mullah, N. & Zalipsky, S. Direct measurement of a tethered ligand-receptor interaction potential. *Science* **275,** 820–822 (1997).
22. Bauer, M. *et al.* Membrane insertion of sliding anchored polymers. *Soft Matter* **9,** 1700–1710 (2013).
23. Kuhl, T. L., Leckband, D. E., Lasic, D. D. & Israelachvili, J. N. Modulation of interaction forces between bilayers exposing short-chained ethylene-oxide headgroups. *Biophys. J.* **66,** 1479–1488 (1994).
24. Helm, C. A., Knoll, W. & Israelachvili, J. N. Measurement of ligand receptor interactions. *Proc. Natl Acad. Sci. USA* **88,** 8169–8173 (1991).
25. Harries, D., Rau, D. C. & Parsegian, V. A. Solutes probe hydration in specific association of cyclodextrin and adamantane. *J. Am. Chem. Soc.* **127,** 2184–2190 (2005).
26. Cohen-Tannoudji, L. *et al.* Measuring the kinetics of biomolecular recognition with magnetic colloids. *Phys. Rev. Lett.* **108,** 301 (2008).
27. Kékicheff, P. in *Electrostatic Effects in Soft Matter and Biophysics* Vol. 46 (eds Holm, C., Kékicheff, P. & Podgornik, R.) 205–282 (Kluwer, 2001).
28. Israelachvili, J. N. Thin film studies using multiple-beam interferometry. *J. Colloid Interface Sci.* **44,** 259–272 (1973).
29. Derjaguin, B. V. Theorie des Anhaftens kleiner Teilchen. *Kolloid Z* **69,** 155–164 (1934).
30. Cubitt, R. & Fragneto, G. D17: the new reflectometer at the ILL. *Appl. Phys. A* **74,** 329–331 (2002).
31. Fragneto, G., Thomas, R. K., Rennie, A. R. & Penfold, J. Neutron reflection from hexadecyltrimethylammonium bromide adsorbed on smooth and rough silicon surfaces. *Langmuir* **12,** 6036–6043 (1996).
32. Koenig, B. W. *et al.* Neutron reflectivity and atomic force microscopy studies of a lipid bilayer in water adsorbed to the surface of a silicon single crystal. *Langmuir* **12,** 1343–1350 (1996).
33. Heavens, O. *Optical Properties of Thin Films* (Butterworth, 1955).
34. Derjaguin, B. V. & Landau, L. Theory of the stability of strongly charged lyophobic sols and the adhesion of strongly charged particles in solutions of electrolytes. *Acta Phys. Chim. USSR* **14,** 633–662 (1941).
35. Verwey, J. W. & Overbeek, J. T. *Theory of the Stability of Lyophobic Colloids* (Elsevier, 1948).
36. Chan, D. Y. C., Pashley, R. M. & White, L. R. A simple algorithm for the calculation of the electrostatic repulsion between identical charged surfaces in electrolyte. *J. Colloid Interface Sci.* **77,** 283–285 (1980).
37. Shubin, V. E. & Kékicheff, P. Electrical double layer structure revisited via a surface force apparatus: mica interfaces in lithium nitrate solutions. *J. Colloid Interface Sci.* **155,** 108–123 (1993).

Acknowledgements

Support from the Agence Nationale de la Recherche under programme ANR-07-Nano-016, and complementary support from Labex NIE 11-LABX-0058-NIE (Investissement d'Avenir programme ANR-10- IDEX-0002-02) are gratefully acknowledged. C.M.M. acknowledges support from the MPIP in Mainz and from CNPq under PVE 400997/2014-2.

Author contributions

M.B and C.F. synthesized and assembled the STL construct; M.B., C.F., T.C. and J.D. performed and interpreted reflectivity measurements; M.B. and P.K. prepared SFA coated surfaces and P.K. performed SFA measurements; J.I. improved key SFA features for preparing and conducting experiments; M.B., P.K. and C.M.M. quantitatively modelled SFA results; J.D. and C.M.M. designed and conducted the project; C.M.M. and P.K. wrote the paper; all authors commented and reviewed the manuscript.

Additional information

Supplementary Information accompanies this paper at http://www.nature.com/naturecommunications

Competing financial interests: The authors declare no competing financial interests.

Reprints and permission information is available online at http://npg.nature.com/reprintsandpermissions/

How to cite this article: Bauer, M. *et al.* Sliding tethered ligands add topological interactions to the toolbox of ligand–receptor design. *Nat. Commun.* 6:8117 doi: 10.1038/ncomms9117 (2015).

Supplementary Figures

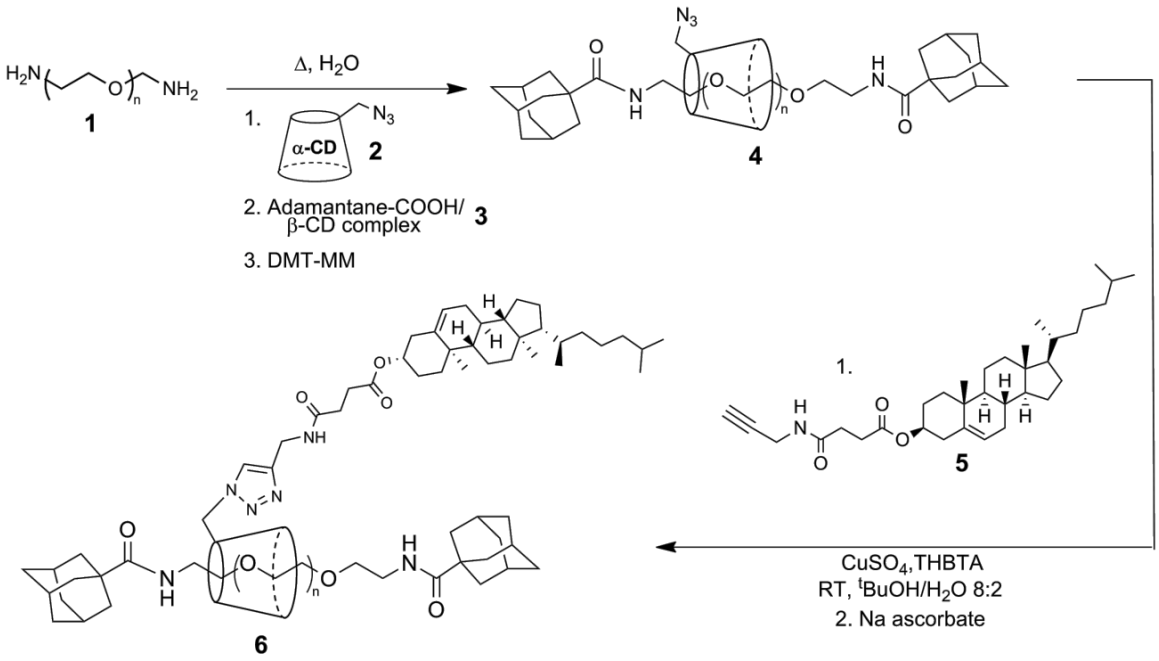

Supplementary Fig. 1. Two-step synthesis of the STL **6**.

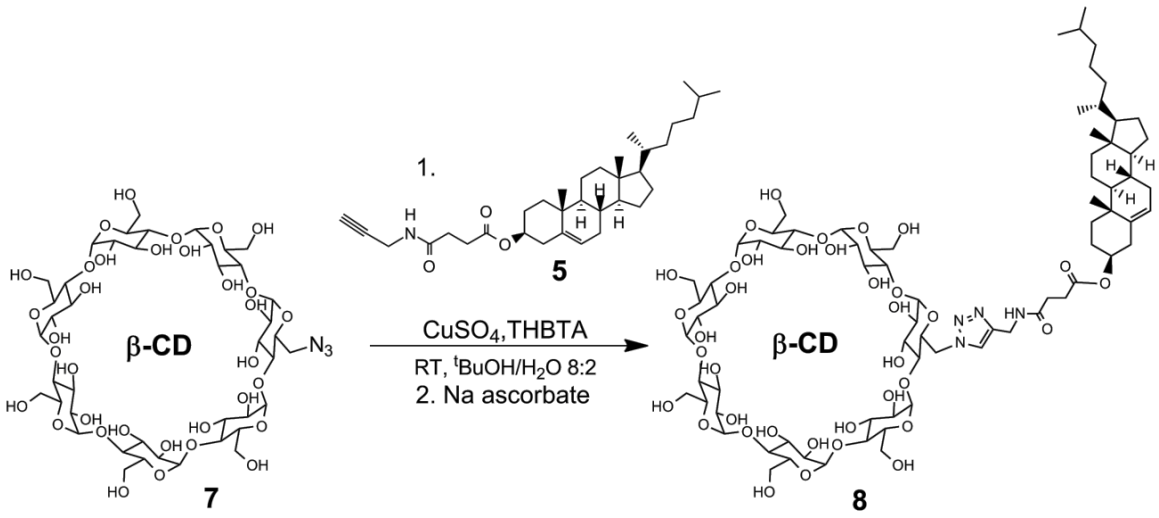

Supplementary Fig. 2. Synthesis of the cholesteryl β-CD receptor **8**.

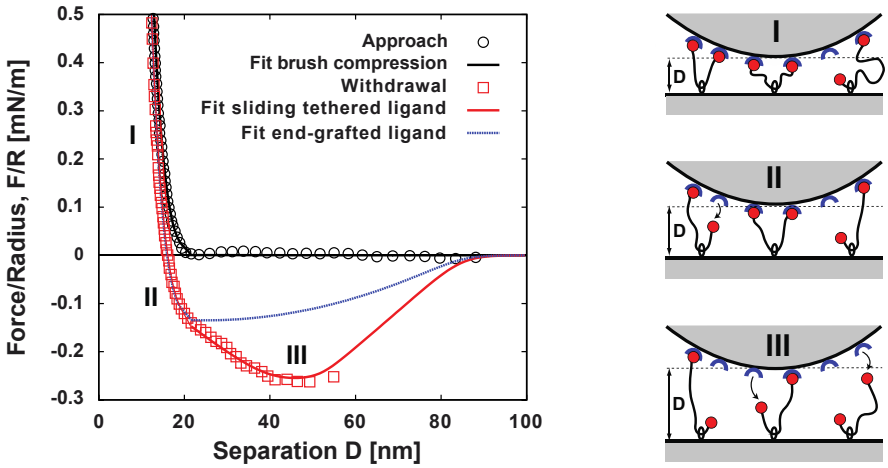

Supplementary Fig. 3. Comparison between two different fits for the pullout experiment with STLs. In blue, best-fit assuming only chain stretching and detachment. In red, the result of fitting with the interconversion mechanism. Note that the almost linear reinforcement of the attractive potential middle range can only be explained by interconversion.

Supplementary Tables

Name	Formula	Molar Mass [g/mol]	Provider
(+)-Sodium-L-ascorbate	$C_6H_7NaO_6$	198.11	Sigma
1-Adamantane carboxylic acid	$C_{11}H_{16}O_2$	180.24	Aldrich
4-Dimethylaminopyridine (DMAP)	$C_7H_{10}N_2$	122.17	Fluka
DMT-MM	$C_{10}H_{17}ClN_4O_3$	276.72	Aldrich
Acetone	CH_3COCH_3	58.08	Sigma-Aldrich
β-CD	$C_{42}H_{70}O_{35}$	1134.98	Wacker
tert-Butanol	$(CH_3)_3COH$	74.12	Fluka
Chloroform	$CHCl_3$	119.38	Sigma-Aldrich
Cholesteryl-hemisuccinate	$C_{31}H_{50}O_4$	486.74	Sigma
Copper(II) sulfate	$CuSO_4$	159.61	Riedel-de Haën
Deuterochloroform	$CDCl_3$	120.38	Eurisotop (France)
Diethylether	$(CH_3CH_2)_2O$	74.12	Sigma-Aldrich
Dimethylsulfoxide-D6 (DMSO-D6)	C_2D_6SO	84.17	Sigma
Methanol	CH_3OH	32.04	Sigma-Aldrich
α-CDN_3	$C_{36}H_{59}N_3O_{29}$	997,86	Biocydex (France)
β-CDN_3	$C_{42}H_{69}N_3O_{34}$	1160,00	own laboratory
bis-amino-PEG-10kD	$H_2N(C_2H_4O)_{222}C_2H_4NH_2$	10000	Aldrich
Propargylamine	$HC_3H_2NH_2$	55.08	Sigma-Aldrich
p-Toluenesulfonic anhydride	$(CH_3C_6H_4SO_2)_2O$	326.38	Sigma-Aldrich

Supplementary Table 1. Chemicals used for the synthesis.

system	h_0 [nm]	p_0h_0 [mN/m]	σ_{brush} [nm^{-2}]	A [nm^2]	$\bar{N}$	PDI
STL/β-CD	14.3	5.0	0.041	22	222	1.25
STL/DPPC	14.0	4.3	0.039	26	222	1.25

Supplementary Table 2. Approach curves displayed in Figure 3 were computed using the MWC model for compression of polymer brushes corrected for polydispersity. The polymer density, σ_{brush}, is calculated from $\sigma_{brush} = (h/a)^3 N^{-3} (\pi^2/12) a^{-2}$ with the size of an ethylene glycol monomer a = 0.35 nm [1]. The available area per polymer chain is $A = \sigma^{-1}$.

system	D^{min} [nm]	h_0 [nm]	N	$\frac{\sigma_N}{\sigma}$ [%]	$\frac{\sigma_{N/2}}{\sigma}$ [%]	f_0 [k_BT/a]
STL/β-CD	7.7±0.1	14.3±0.1	640	0.40	0.079±0.001	2.6±0.1
	11.0±0.1	14.3±0.1	630	0.41	0.070±0.001	2.6±0.1
	13.9±0.1	14.3±0.1	630	0.50	0.032±0.001	2.6±0.1
	17.1±0.1	14.3±0.1	630	0.19	0	-

Supplementary Table 3. Results from fitting the withdrawal curves displayed in Figure 8 using equation (1) in the main text. For all fits the binding energy was set to 10 k_BT, which is the complexation energy of β-CD and adamantane [2,3]. The distance for maximum compression at each run is denoted by D^{min}, N is the number of monomers of the bridging polymers, $\frac{\sigma_N}{\sigma}$ is the fraction of single bridging polymers (the strands) calculated respectively to the total surface density σ 0.044 nm^{-2} (23 nm^2 per each tethered ligand molecule), and $\frac{\sigma_{N/2}}{\sigma}$ is the double bridging polymer fraction (the loops). Significant variations in the accuracy of the fittings can be seen for deviations of the parameters N, $\boldsymbol{\sigma_N}$ and $\boldsymbol{\sigma_{N/2}}$ larger than a few percent. Note that the low fraction of chains involved in bridging and looping implies that no significant modifications to the repulsive part of the profile can be detected upon separation. Values of the measured friction coefficients correspond to those of a bead of a size of a monomer moving in a liquid ten times more viscous than water.

Layer	Parameters	Cholesteryl β-CD	STL
Water	Thickness [nm]	0.7 ± 0.1	0.5_5 ± 0.1
	SLD [Å^{-2}]	-	-
	Water [v/v%]	100	100
	Roughness [nm]	0.5 ± 0.1	0.6± 0.1
Heads DSPE	Thickness [nm]	0.6 ± 0.1	0.6_5 ± 0.1
	SLD [Å^{-2}]	2.6	2.6
	Water [v/v%]	40 ± 5	35 ± 5
	Roughness [nm]	0.5_5 ± 0.2	0.6 ± 0.2
Tails	Thickness [nm]	3.7 ± 0.1	3.9 ± 0.1
	SLD [Å^{-2}]	-0.3	-0.3
	Water [v/v%]	14 ± 5	7 ± 5
	Roughness [nm]	0.5_5 ± 0.2	0.7 ± 0.2

Heads DPPC/CD	thickness [nm]	$0.9_8 \pm 0.1$	$0.9_6 \pm 0.1$
	SLD [$Å^{-2}$]	1.8	1.8
	Water [v/v%]	35 ± 5	25 ± 5
	Roughness [nm]	$0.5_5 \pm 0.2$	$0.8_5 \pm 0.2$
PEG	Thickness [nm]	-	13.0 ± 1.0
	SLD [$Å^{-2}$]	-	0.6
	Volume fraction Φ_0	-	0.08 ± 0.02
	Roughness [nm]	-	0.8 ± 0.2

Supplementary Table 4. Neutron reflectivity results for supported bilayers with a first monolayer DSPE as well as a second mixed monolayer DPPC/cholesteryl β-CD and DPPC/STL, respectively. The obtained results for the polymer layer yield in a STL surface density $\sigma = 0.051$ nm^{-2}, which is in good agreement with the SFA data (see Supplementary Table 2).

Supplementary Methods

1. Synthesis

1.1. Synthesis of the STL

The STL **6** is synthesized in two steps starting from poly(ethylene glycol) bis(amine) **1** (Supplementary Fig. 1). In the first step polyrotaxanes with a controlled, very low threading ratio are formed with azido α-CD (6I-azido-6I-deoxy-cyclomaltohexaose) **2**, threaded onto the PEG chains in water. A small number of CDs per chain is achieved by forming the PEG/CD inclusion complex at high temperatures, which additionally provides sufficient solubility of the poorly soluble modified CD as previously reported [4]. However the reported capping reaction requires the prior preparation of a water soluble blocked isocyanate to yield the blocking urea. Capping reactions in water are not numerous [5]. In order to get a more versatile pathway, we turned to Kunishima's method to form carboxamide using DMT-MM (4-(4,6-Dimethoxy-1,3,5-triazin-2-yl)-4-methylmorpholinium chloride) in protic solvents [6,7]. This was introduced in rotaxane chemistry by Easton & Coll. [8] and more recently used with polyrotaxanes in a mixture of DMSO and water by the group of Yui [9]. The insoluble adamantane carboxylic acid was rendered water soluble as a β-CD complex **3**. It was then reacted in situ with the pseudo-polyrotaxane formed from **1** and **2**. It was observed that the same number of CDs per chain was obtained in the chosen complexation conditions with both capping methods. The adamantane terminated polyrotaxane 4 was thus obtained by simple dialyses in 25% yield.

The final product is obtained by attaching a cholesteryl succinic acid propargylamide **5** to the polyrotaxane **4** via a click chemistry approach, adapting the method recently reported by Finn & Coll. [10] to afford the STL **6**. The cholesteryl succinic acid propargylamide **5** is previously synthesized in one step from propargylamine and cholesteryl hemisuccinate activated as a toluene sulfonic mixed anhydride [11] according to Mukaiyama & Coll. [12]. All products were verified by NMR recorded on a Bruker DMX300 spectrometer and a BB probe. NMR data were processed and plotted using MestRe-C. Extensive dialyses remove salts and soluble small molecules. Filtration removes insoluble matter. NMR signals include only peaks accounting for the polymer and threaded modified α-CD.

1.2. Synthesis of the cholesteryl β-CD receptor

The cholesteryl β-CD **8** is obtained in one step from azido β -CD (7I-azido-7I-deoxy-cyclomaltoheptaose) **7** with the same click chemistry approach already mentioned in section 1.1. using cholesteryl succinic acid propargylamide **5**. Small compounds **5** and **8** show single spot in TLC and no extra peak in NMR.

1.3. Materials

1.3.1 Used Chemicals

The chemicals and solvents used throughout the synthesis are listed in Supplementary Table 1.

1.3.2 Synthesis of the 1-adamantane carboxylic acid/β-CD complex 3

700 mg (0.62 mmol, 1eq) β-CD were dissolved in 50 ml of millipore water, sonicated for 20 min and then heated to 70°C while stirring. Likewise 450 mg (2.5 mmol, 4eq) of 1-adamantane carboxylic acid were dissolved in 50 ml of acetone and added slowly to the β-CD solution via a dropping funnel. Then the transparent mixture was sonicated for 45 min and left stirring at 70°C for 3h to completely evaporate the acetone. 30 ml of water were added to the now turbid mixture. Then it was filtered with a 1 µm fiber glass filter and washed several times with Millipore water. The transparent solution was freeze dried to give **3**.

Yield: 710 mg, (87 %)

^{1}H-NMR (300MHz, DMSO-D6): 5.8 (14H, -OH-1 and -OH-2 CD); 4.8 ppm (7H, H-1 CD); 4.45 ppm (7H, -OH-6 CD); 2.5 ppm (residual H_2O); 1.95 ppm (3H, -C-H adamantane); 1.78 ppm (6H, -CH_2-CCOOH adamantane); 1.65 ppm (6H, -CH_2-CH adamantane)

1.3.3 Synthesis of the polyrotaxane 4

100 mg (10 µmol, 1eq) α,ω-diamino PEG **1** (N = 222, MW = 10000 g/mol) was dissolved in 3.4 ml millipore water and 150 mg (150 µmol, 15eq) α-CDN_3 **2** were added. The transparent solution was left stirring at 70°C for 2h. Then at first 55 mg (40 µmol, 4eq) 1-Adamantanecarboxylic acid/β-CD complex **3** and subsequently 12 mg (40 µmol, 4eq) DMT-MM were added to the solution, which was left stirring at 70°C for 12h. Finally the mixture was diluted with 15 ml of millipore water and dialysed (cut-off 2000 g/mol) four times with 1.5l of millipore water at 50°C. The transparent solution is freeze dried to give **4**.

Yield: 30 mg (25%)

^{1}H-NMR (300MHz, $CDCl_3$): 7.35 ppm (2H, NHCO- stopper); 5.6 ppm - 5.4 ppm (12H, OH-2 and OH-3 CD); 4.8 ppm (6H, H-1 CD); 4.45 ppm (6H, OH-6 CD); 3.1-3.9 (nH, -OCH_2CH_2-PEG and H-2, H-5, CH_2-6 CD); 2.5 ppm (residual H_2O); 1.9 ppm (6H, CH adamantane); 1.7 (24H, CH_2 adamantane)

1.3.4 Synthesis of cholesteryl succinic acid propargylamide 5

2.5 g (5.1 mmol, 1.1 eq) of cholesterol-hemisuccinate, 1.81 g (5.6 mmol, 1.3 eq) of toluenesulfonic anhydride and 1.26 g (10 mmol, 2.2 eq) of DMAP were dissolved in 25 ml of $CHCl_3$ and after 15 min 0.26 g (4.6 mmol, 1 eq) propargylamine were added. After 1.5h the mixture was quenched with 3 ml of saturated $NaHCO_3$ solution. The solution was extracted with ethyl acetate and the combined organic layers were washed two times with 50 ml of saturated $NaHCO_3$, two times with 50 ml of brine and the organic layer was dried over anhydrous Na_2SO_4. The crude product was purified by recrystallization in ethyl acetate and freeze dried from cyclohexane to give **5**.

Yield: 1.25 g (55 %)

^{1}H-NMR (300MHz, $CDCl_3$): 6.2 ppm (1H, -NHCO-); 5.35 ppm (1H, H-6 Cholesterol); 4.6 ppm (1H, H-3 Cholesterol); 4.0 ppm (2H, -CH_2 propargyl); 2.2 ppm (1H, H-alkyne); 0.65 ppm (9H, -CH_3 cholesterol)

1.3.5 Synthesis of the STL 6

Prior to the experiment solutions of $CuSO_4$ (c = 0.13 mol/l) and a THBTA (c = 63 mmol/l) are prepared with Millipore water. The polyrotaxane **4** (30 mg, 2.8 µmol, 1eq) and the cholesteryl succinic acid propargylamide **5** (6 µmol, 2eq (per azide)) were dissolved in a mixture of 1.5 ml tert-BuOH/Millipore water 8:2, sonicated for 5 min and heated for several minutes to provide for complete dissolution of the compounds. Then the ligand solution (1 µmol, 0.3 eq) and the CuSO4 solution (0.2 µmol, 0.06 eq) were added to the mixture to give a transparent solution. Sodium ascorbate (2.5 µmol, 0.8 eq) was added and the solution was left stirring for 4h at room temperature. The transparent solution was diluted with 5 ml of Millipore water and dialyzed (cut-off 2000 g/mol) twice with 2l of millipore water for 24h and freeze dried. The crude product was taken up in 5 ml of ether and centrifuged 3 times to eliminate the residual cholesteryl succinic acid propargylamide. The residue was dissolved in 10 ml of tert-BuOH/H2O 8:2 and freeze dried to give **6**.

Yield: 13 mg (50%)

^{1}H-NMR (300MHz, $CDCl_3$): 8.3 ppm (1H, NHCO- succinyl); 7.8 ppm (1H, H-triazol); 7.8 ppm (2H, NHCO- stopper); 5.6 ppm - 5.4 ppm (12H, OH-2 and OH-3 CD); 5.3 ppm (1H, CH sp2 cholesterol); 5.0 ppm (1H, H-1 modified glucose unit CD); 4.8 ppm (5H, H-1 CD); 4.5 ppm (6H, OH-6 CD); 3.1-3.9 (nH, -OCH_2CH_2- PEG and H-2, H-5, CH2-6 CD); 2.5 ppm (residual H2O); 1.9 ppm (6H, CH adamantane), 1.7 (24H, CH_2 adamantane); 1.8 - 0.8 ppm (H cholesteryl moiety); 0.65 ppm (9H, -CH_3 cholesterol)

1.3.6 Synthesis of the cholesteryl β-CD 8

Prior to the experiment solutions of $CuSO_4$ (c = 0.13 mol/l) and THBTA (c = 63 mmol/l) were prepared with Millipore water. 47 mg (40 µmol, 1eq) β-CDN_3 and 28 mg (56 µmol, 1.4eq) cholesteryl succinic acid propargylamide **5** were introduced into 16 ml of tert-butanol and sonicated for 10 min. Then 228 µl (13 mg, 30 µmol, 0.75 eq) of the THBTA solution and 72 µl (0.77 mg, 5 µmol, 0.1eq) of the $CuSO_4$ solution were mixed in 3.7 ml of water added to the mixture to give a slightly turbid suspension. 40 mg (200 µmol, 5eq) of sodium ascorbate were put into the solution and the mixture was stirred for 1h at room temperature. In the next step the compound was centrifuged three times in 10 ml of buffer/EDTA solution (2 mg EDTA in phosphate buffer pH = 6.5) and three times in 3 ml of acetone. The compound was taken up in 5 ml of Millipore water and freeze dried to give **8** (Supplementary Fig. 2).

Yield: 62 mg (90 %)

^{1}H-NMR (300MHz, DMSO-D6): 8.30, 8.27 ppm (s, 1H, -NHCO-); 7.83, 7,66 ppm (s, 1H, H-triazol); 5.6 ppm - 5.4 ppm (14H, OH-2 and OH-3 CD); 5.0 ppm (1H, H-1 modified glucose unit CD); 4.8 ppm (6H, H-1 CD); 4.4 ppm (7H, OH-6 CD); 3.2-3.7 (H-2 and H-5, CH_2-6 CD); 2.5 ppm (residual H_2O), 2 - 0.8 ppm (H's of cholesteryl moiety); 0.65 ppm (9H, -CH3 cholesterol)

2. Direct Force Measurements (SFA)

2.1. A note on the bare bilayer thicknesses

Note that the added thickness of the two decorated bilayers in Fig. 4 of the main text is slightly larger, by 0.2 nm only, than that of the corresponding bare bilayers. Since the zero reference distance for all force-distance profiles is defined at the contact of the two decorated bilayers as in Fig.1 of main text, some precisions must be added here. First, one can remark that at very short separations the compliance of the steric repulsion is smaller in the presence of STLs compared to the situations where no polymer is present (compare Fig. 4, Fig. 5 and Fig. 6 of the main article). If a contact value can be easily defined for Fig. 6, as the steric repulsion vs. separation appears almost vertical, defining contact values for other cases is not as straightforward. For Fig. 5 this "contact" (9.6±0.2 nm) corresponds to the thicknesses of the two bilayers when they are brought to contact, while it would be slightly larger by about 0.2 nm for Fig.4 and 0.1-0.2 nm for Fig. 5. For these latter situations the contact value is defined by extrapolation from the slope of the steric repulsion compliance, since we have avoided applying too large loads in order not to damage the structure of the decorated bilayers. In any case, the additional 0.2 nm cannot be interpreted as a thickness layer due to compression of the polymer at infinite loads. It is more likely due to the rearrangement of the ß-CDs in the presence of STLs, which, under high loads, are likely to re-orient and protrude slightly from the bilayer, as seen in [4].

2.2 A note on the role of ligand polydispersity on the attractive forces

We should stress that while compression curves are well explained by a polymer length distribution with average polymerization index N=220 and PDI=1.25 (note that our PDI is well within the bounds provided by Sigma Aldrich that states that PDI < 1.3 for these samples), chains with N~ 600 contribute mostly to the withdrawal forces. This calls for two remarks. First, such an amount of large chains exists indeed in the distribution: for a Flory-Schulz distribution with average length 220 and PDI=1.25, there are ~ 0.34 % of the chains with N>630, comparable to the values in Supplementary Table 3. Moreover, as explained above, our preparation of the STL constructs involves a dialysis step that is likely to skew the original polymer distribution towards the larger chains. Secondly, the predominance of large chains contributing to the attractive forces is likely to be a direct consequence of the conditions for bridging. Indeed, for a given distance at contact between the two opposing surfaces, the probability of bridging increases with the size of the chains.

Supplementary References

(1) Moore, N. W. & Kuhl, T. L. Bimodal polymer mushrooms: Compressive forces and specificity toward receptor surfaces. *Langmuir* **22** (20), 8485-8491 (2006).

(2) Auletta, T., de Jong, M. R., Mulder, A., van Veggel, F. C. J. M., Huskens, J., Reinhoudt, D. N., Zhou, S., Zapotoczny, S., Schönherr, H., Vancso, G. J. & Kuipers, L. ß-Cyclodextrin host-guest complexes probed under thermodynamic equilibrium: Thermodynamics and AFM force spectroscopy. *J. Am. Chem. Soc.* **126** (5), 1577-1584 (2004)

(3) Harries, D., Rau, D. C. & Parsegian, V. A. Solutes probe hydration in specific association of cyclodextrin and adamantane. *J. Am. Chem. Soc.* **127** (7), 2184-2190 (2005).

(4) Bauer, M. Bernhardt, M., Charitat, T., Kékicheff, P., Fajolles, C. Fragneto, G., Marques, C. M. & Daillant, J. Membrane insertion of sliding anchored polymers *Soft Matter* **9**, 1700-1710 (2013).

(5) Fleury, G., Brochon, C., Schlatter, G., Bonnet, G., Lapp, A. & Hadziioannou, G., Synthesis and characterization of high molecular weight polyrotaxanes: towards the control over a wide range of threaded alpha-cyclodextrins. *Soft Matter* **1** (5), 378-385 (2005).

(6) Kunishima, M., Kawachi, C., Morita, J., Terao, K., Iwasaki, F. & Tani, S. 4-(4,6-dimethoxy-1,3,5-triazin-2-yl)-4-methyl-morpholinium chloride: An efficient condensing agent leading to the formation of amides and esters. *Tetrahedron* **55** (46), 13159-13170 (1999).

(7) Kunishima, M., Kawachi, C., Hioki, K., Terao, K. & Tani, S. Formation of carboxamides by direct condensation of carboxylic acids and amines in alcohols using a new alcohol- and water-soluble condensing agent: DMT-MM. *Tetrahedron* **57**, 1551-1558 (2001).

(8) Maniam, S., Cieslinski, M. M., Lincoln, S. F., Onagi, H., Steel, P. J., Willis, A. C. & Easton, C. J. Molecular Fibers and Wires in Solid-State and Solution Self-Assemblies of Cyclodextrin [2]Rotaxanes. *Org. Lett.* **10** (10), 1885-1888 (2008).

(9) Hyun, H. & Yui, N. Mono-, Di-, or Triazidated Cyclodextrin-Based Polyrotaxanes for Facile and Efficient Functionalization via Click Chemistry. *Macromol. Rapid Commun.* **32**, 326-331 (2011).

(10) Hong, V., Presolski, S. I., Ma, C. & Finn, M. G. Analysis and Optimization of Copper-Catalyzed Azide–Alkyne Cycloaddition for Bioconjugation. *Angew. Chem. Int. Ed.* **48** (52), 9879-9883 (2009).

(11) Bauer, M., Fajolles, C., Charitat, T., Wacklin, H. & Daillant, J. Amphiphilic Behavior of New Cholesteryl Cyclodextrins: A Molecular Study. *J. Phys. Chem. B* **115**, 15263-15270 (2011).

(12) Funasaka, S., Kato, K. & Mukaiyama, T. Highly efficient method for the synthesis of carboxamides from carboxylic acids and amines using benzenesulfonic anhydride (BSA). *Chem. Lett.* **36**, 1456-1457 (2007).